

# Automated Design and Optimization of Distributed Filtering Circuits via Reinforcement Learning

Peng Gao, Tao Yu, Fei Wang, and Ru-Yue Yuan

**Abstract**—Designing distributed filtering circuits (DFCs) is complex and time-consuming, with the circuit performance relying heavily on the expertise and experience of electronics engineers. However, manual design methods tend to have exceedingly low-efficiency. This study proposes a novel end-to-end automated method for fabricating circuits to improve the design of DFCs. The proposed method harnesses reinforcement learning (RL) algorithms, eliminating the dependence on the design experience of engineers. Thus, it significantly reduces the subjectivity and constraints associated with circuit design. The experimental findings demonstrate clear improvements in both design efficiency and quality when comparing the proposed method with traditional engineer-driven methods. In particular, the proposed method achieves superior performance when designing complex or rapidly evolving DFCs. Furthermore, compared to existing circuit automation design techniques, the proposed method demonstrates superior design efficiency, highlighting the substantial potential of RL in circuit design automation.

**Index Terms**—Filtering circuit, electronic design automation, circuit optimization, reinforcement learning.

## I. INTRODUCTION

**D**ISTRIBUTED filtering circuits (DFCs) are designed by combining components such as resonators. Numerous domains, ranging from complex cellular networks to expansive satellite communication systems, rely heavily on these circuits [1]–[3]. In particular, in high-frequency scenarios, electronic components often exhibit impedance characteristics. An efficient DFC plays a crucial role in facilitating rapid signal transmission and clear signal reception. In contrast to a low-frequency analog circuit design that treats each component as an independent unit with a specific functionality, a DFC design involves interdependent components. The geometric parameters and spatial relationships of each component in DFCs can significantly impact the functionalities of other components. Moreover, the geometric parameters of one component can be influenced by other components [4], [5]. This interdependence among components can lead to unexpected resonances and scattering phenomena in DFCs.

In DFC design, squares [6] or circular resonators [4] typically serve as the fundamental building blocks. These resonators can selectively amplify or suppress specific signal frequencies based on the design requirements. Resonance occurs when the frequency of the input signal matches the resonant frequency of the resonator. The manual design of

P. Gao and T. Yu are with the School of Cyber Science and Engineering, Qufu Normal University, Qufu, Shandong 273165, China.

F. Wang is with the School of Integrated Circuits, Harbin Institute of Technology, Shenzhen, Guangdong 518055, China.

R.-Y. Yuan is an individual researcher.

DFCs by electronic engineers is an intricate process, often involving the fulfillment of multifaceted requirements. The initial design scheme is proposed by an electronic engineer by considering the expected frequency passband of the filtering circuit. Subsequently, the engineer generally selects a filtering circuit template composed of resonators and iteratively adjusts and optimizes the geometric parameters of these resonators within the template. Moreover, engineers frequently conduct electromagnetic simulations via commercial software tools to predict signal-resonator interactions and those among the resonators themselves. However, this design process is time-consuming and resource intensive, and is predominantly dependent on the expertise and experience of electronics engineers.

With the continuous evolution of artificial intelligence (AI), reinforcement learning (RL) has emerged as an effective tool for solving decision-making problems. During RL, the continuous interaction between an intelligent agent and its applied environment enables the agent to learn and optimize strategies through an iterative trial-and-error approach. Hong et al. noted that different filtering circuits can be designed by altering the number and geometric parameters of resonators [4]. Leveraging this capability, we consider the design and optimization of DFCs as sequential decision-making tasks. The intelligent agent optimizes the performance of the DFCs by modifying the geometric parameters. However, it is challenging to design a DFC that fulfills the performance requirements. The primary obstacle is the highly complex nonlinear relationship between the geometric parameters of the circuit and the performance requirements. In most cases, the resonators must be positioned without overlap.

In this study, we developed a novel end-to-end automated method for DFC design to address the aforementioned problems. The main contributions of this study are outlined below:

- 1) Introduction of an RL-based DFC design and optimization (RLDFCDO) method that automatically adjusts the geometric parameters of individual resonators to optimize circuit performance.
- 2) Implementation of the best reward initialization (BRI) method, facilitating the design of initial circuit layouts compliant with performance requirements yet non-optimal.
- 3) Introduction of the state evaluator (SE) method to evaluate the performance of the circuits designed by RLDFCDO and BRI.
- 4) Utilization of an invalid action penalty (IDP) mechanism that enables RLDFCDO to avoid invalid design schemes (overlapping the placement of resonators), thereby in-

creasing the probability of intelligent agents learning superior circuit design schemes.

5) Provision of an end-to-end DFC design and optimization solution. A filtering circuit design that satisfies the stipulated requirements can be obtained by inputting the expected frequency passband.

The rest of the paper is organized as follows: we first introduce the related works in Section II, then show how to design and optimize DFCs via reinforcement learning in Section III, next conduct extensive experiments in Section IV to evaluate the proposed method, and finally draw a conclusion in Section V.

## II. RELATED WORKS

### A. Learning-Based Circuit Design and Optimization

Historically, circuit design and optimization have presented challenges, stimulating innovative methodologies. Colleran *et al.* introduced geometric programming to optimize phase-locked loop circuits [7]. Liu *et al.* proposed an analog circuit optimization approach based on a hybrid genetic algorithm (GA) [8], showcasing the potential of GAs in this domain. With the evolution of machine learning technology, the direction of research on circuit design and optimization methods has gradually shifted. Wang *et al.* combined sparse regression and polynomial optimization to efficiently synthesize analog circuits [9]. McConaghy *et al.* [10] and Lourencco *et al.* [11] further explored the potential of GAs in circuit optimization. McConaghy *et al.* focused on trustworthy genetic programming-based synthesis using hierarchical domain-specific building blocks, while Lourencco *et al.* introduced GENOM-POF, a multi-objective evolutionary synthesis approach with corner validation. Subsequently, Lyu *et al.* presented a series of Bayesian optimization-based analog circuit design methods [12]–[14], highlighting their efficacy in handling uncertainty and optimizing complex design spaces. He *et al.* investigated end-to-end learning for distributed circuit design [15] and graph neural networks (GNNs) [5], demonstrating the potential of deep learning techniques for abstracting complex state-space information and optimizing circuit layouts. Furthermore, Cao *et al.* [16] and Feng *et al.* [17], [18] employed complex neural networks and parameter modeling of transfer functions. They emphasized the significance of accurate modeling in ensuring the optimized design and performance of microwave components. Recent studies have highlighted the immense potential of deep learning in automated circuit design. For instance, some researchers have employed deep neural networks (DNNs) based on Thompson sampling for efficient multi-objective optimization [19]. Others have proposed an RL-based quantum circuit optimizer [20], employing gradient-based supervised learning algorithms to train a design agent to satisfy the threshold specifications of analog circuits [21].

### B. RL for Sequential Decision-Making Tasks

Over the past decade, significant advancements have made RL algorithms adept at effectively addressing challenging sequential decision-making problems. Early RL research focused primarily on value-based methods. The value function serves

as a core concept for estimating the expected return of an agent to a given state or after taking a specific action. Techniques such as Q-learning [22] represent the value function in a tabular manner, making action decisions by maximizing this function. Although table-based methods are effective in small, discrete environments, they struggle to scale up to larger or continuous state spaces. Linear function approximation methods such as tile coding enable RL to handle large state spaces [23], [24]. However, tile coding has some fatal flaws, primarily in its fixed and non-learning-capable tiles and the difficulty involved in representing complex state features through linear combinations of tiles. These drawbacks of tile coding and other linear approximation methods have motivated scholars to explore nonlinear function approximations, such as neural networks [25]. Nevertheless, early shallow neural networks could not easily achieve the representational power and stability attained in traditional RL. A major turning point in this field was the introduction of deep RL (DRL), which automatically extracts useful state features by utilizing DNNs. Neural networks enable the complex abstraction modeling of complex state spaces. End-to-end training enables neural networks to adapt to RL problems. DRL has paved the way for new possibilities in addressing a wide array of sequential decision-making challenges. It primarily employs DNNs for functional approximation. Deep Q-networks (DQNs) combine key methods such as Q-learning, DNNs, and experience replay [26], enabling RL agents to master complex visual environments and achieve human-level performance. Double DQN [27] and dueling architectures [28] have further improved the performance of DRL. DRL has been applied to various sequential decision-making tasks, including robotics [29], games [30], and recommendation systems [31]. Another crucial approach is the actor-critic method [32], which requires separate maintenance of the policy and value functions. The asynchronous advantage actor-critic approach [33] achieved state-of-the-art results by parallelizing experience collection. Policy gradient techniques, such as trust region policy optimization (TRPO) [34] and proximal policy optimization (PPO) [35], directly optimize neural network policies while ensuring monotonic yet stable training improvement. Bueno *et al.* [36] introduced RL in large-scale photonic recurrent neural networks, demonstrating outstanding predictive performance in the Mackey–Glass chaotic time series. Kaufmann *et al.* [37] proposed Swift, an autonomous drone racing system that utilizes real-world data and fine-tunes the model using the PPO algorithm. Kulkarni *et al.* [38] explored the decomposition of problems into higher-level abstractions by using hierarchical RL. Recently, RL has displayed extensive potential and made significant strides across various fields. Sugiyama *et al.* [39] investigated the metacognitive processes of motor learning using RL, revealing how humans optimize learning strategies by adjusting learning and retention rates based on feedback. Barata *et al.* [40] applied RL to skin cancer diagnosis, considerably improving the diagnostic sensitivity and accuracy by integrating medical expert preferences with non-uniform reward and penalty mechanisms. Guo *et al.* [41] employed a stochastic subsampling RL method to optimize long-term career path recommendation systems. Regarding

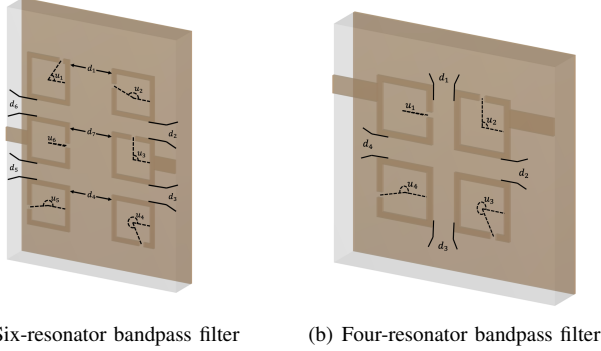


Fig. 1. Examples of distributed filtering circuit templates based on square resonators. In the figure,  $d$  indicate the relative distance between two resonators, and  $u$  represents the counterclockwise angle from the horizontal line to the line connecting the opening position and the center point.

robotics control, Ju *et al.* [42] successfully transferred policies trained in simulation environments to the real world. Kuprikov *et al.* [43] effectively controlled complex laser systems using deep RL, offering new technological pathways for stable pulse generation. These studies showcase the extensive applicability of RL across multiple domains and highlight its remarkable achievements through innovative approaches.

### III. METHOD

A typical DFC comprises parameterized resonators, as depicted in Fig.1. The flowchart shown in Fig.2 illustrates the basic process of optimizing circuit parameters based on a given frequency passband. The geometric parameters of the resonators often determine the filtering circuit performance. We aim to automate the optimization of these geometric parameters based on the expected frequency passband. The optimization process can be modeled as a Markov decision process, wherein an intelligent agent interacts with the environment, performs specific actions impacting it, and receives rewards based on environmental feedback. Through multiple iterations and interactions with the environment, the agent learns an optimal policy that maximizes the long-term cumulative rewards. In DFC design and optimization problems, the environment, state, actions, and reward, correspond to the circuit performance simulation, current geometric parameters of all resonators, changes in the geometric parameters, and circuit performance, respectively.

We employed the PPO algorithm [35] to train the agents. Compared to TRPO [34], PPO offers several advantages, such as simpler implementation, higher and more stable sampling efficiency, and reduced sensitivity to hyperparameter selection. In this study, the optimization problem of the resonator geometric parameters was abstracted as a controllable RL process, establishing a novel optimization workflow for designing DFCs. The proposed method employs computer-based large-scale simulation for rapid iterative parameter optimization. As RL does not rely on the domain expertise and design experience of engineers, it can explore potential design solutions more efficiently than manual methods. Moreover, the approach only requires the specifications of the expected frequency

passband. An RL method capable of automatically designing and optimizing DFCs based to the demands and constraints was implemented by constructing an intelligent agent, a state space, action space, and reward function. For convenience, we describe a design method that utilizes square resonators as the fundamental components of a DFC.

#### A. State Space

In RL methods, the state space directly affects the learning efficacy and is crucial in problem modeling. We designed a two-dimensional (2D) continuous state space to comprehensively reflect the geometric and spatial information of the circuit. A continuous state space effectively represents fine changes in the circuit parameters. In such a state space, different states correspond to minor variations in the circuit, enabling the agent to explore the design space intricately to identify the optimal parameter settings. Moreover, employing a continuous state enables leveraging of the advantages of RL algorithms for exploring optimal solutions within continuous spaces. Furthermore, continuous states naturally handle novel states that are not encountered during training, featuring strong generalization capabilities. The state space employs real-valued vectors to represent the geometric parameters of each resonator in the circuit. Each resonator is characterized by an eigenvector composed of nine parameters: the horizontal position ( $x$ ), vertical position ( $y$ ), side length ( $l$ ) of the square resonator cavity, wall thickness ( $w$ ), horizontal position of the opening ( $gap_x$ ), vertical position of the opening ( $gap_y$ ), gap height ( $gap_h$ ), gap width ( $gap_w$ ), and the counterclockwise angle ( $u$ ) from the horizontal line to the line connecting the opening position and the center point. These parameters reflect critical information regarding the spatial distribution and geometric shape of the resonator, which directly determine the circuit topology. As the resonator size parameters often have a significant impact on the frequency response of the circuit, the state space design should include as many relevant parameters as possible. In a specific implementation, we represent the state space as a matrix, where each row vector corresponds to the feature representation of a resonator. The state matrix is fed into the policy network, where a fully connected NN with two hidden layers is employed to extract and transform the state inputs, generating a high-dimensional abstract representation of the circuit. Compared with a simple state representation, our 2D state space enables more effective learning, leading to more optimal circuit design schemes.

#### B. Action Space

Following state space creation, we designed a corresponding action space. The action space contains a set of actions that can be applied to the current circuit state to search for an optimal design by changing the circuit parameters. We employed a representation of a discrete action space for the design and optimization problem addressed in this study. In complex environments with numerous possible actions, the use of a discrete action space simplifies the learning process and enhances efficiency [44], [45]. This choice was primarily based on the following factors. First, when considering the multitude

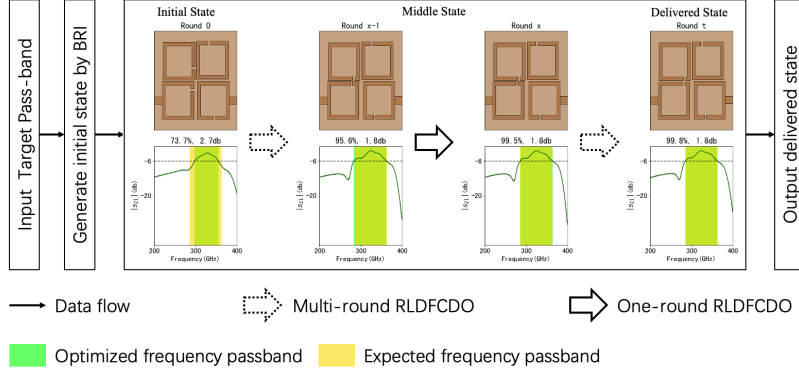


Fig. 2. Schematic of end-to-end design and optimization of DFCs.

of optimizable parameters for the resonators, using a continuous action space burdens the learning process of the policy network, making it difficult to implement effective training. Discrete actions provide clear guidance for the search direction and reduce the learning difficulty. Second, discrete actions are advantageous for implementing a penalty mechanism for invalid actions and for avoiding erroneous designs that are difficult to judge with continuous actions. Moreover, compared with the random fluctuations of continuous actions, discrete actions explicitly represent the range and precision of changes, reducing ineffective randomness and favoring stable learning. Finally, discrete actions can express a richer set of actions through combinations, enhancing the expressive ability.

Based on these considerations, we defined various combinations of discrete actions to optimize the geometric parameters of the resonator. These actions were applied to the specified resonators and could be freely combined to alter the circuit topology. Moreover, we explicitly outlined the effects of different geometric parameters on the circuit performance and appropriately set the variation amplitude for each action. For parameters that have a significant impact, we set small variation ranges, in contrast, we allowed larger variation ranges for parameters less sensitive to minor adjustments. Moreover, we defined different combination actions to simultaneously adjust the different resonator parameters. In the later stages of training, the probability of combination actions is gradually increased for detailed optimization. Since the resonators cannot overlap, the feasibility of the action space is restricted. Therefore, we defined different penalty intensities for invalid actions based on the action range. However, a few invalid designs were allowed to maintain the completeness of the state space. We could rapidly explore the effective state space and develop a strategy for generating high-quality circuits by precisely setting the penalty intensity. In addition, we devised a specific operation wherein invalid actions were randomly executed with a certain probability, and hidden samples were introduced to enhance the generalization capability of the model. Additionally, we expanded the action space by incorporating combined operations that led to more varied changes in circuit topologies.

### C. Reward Design

In RL methods, the reward mechanism is the core driver that guides the training of the model. We specifically crafted a multi-objective, dynamically adjustable reward function to induce the intelligent agent to autonomously optimize the circuit design parameters. The reward function comprises three primary components.

- The first component is the frequency passband overlap.  $IOU = \frac{Pass_t \cap Pass_d}{Pass_t \cup Pass_d}$  is calculated based on the passband  $Pass_d$  of the delivered circuit and the expected passband  $Pass_t$ . This indicator mirrors the quality of the frequency passband coverage of the delivered circuit. A higher IOU signifies a greater overlap between the expected and delivered on-state frequencies.
- The second component is the insertion loss, which measures the signal strength reduction. This loss quantifies the signal transmission efficiency from the input to the output and is generally measured in decibels (dB). In designing radio frequency (RF) and microwave components, a low insertion loss implies that the signal maintains high strength during transmission. We utilized the inverse of the maximum value of the circuit frequency response function as the insertion loss [5]. Design schemes with low losses were also rewarded.
- The third component is the deviation of the central frequency, which reflects the concentration level of the frequency passband response. A smaller deviation indicates that the frequency passbands have more concentrated alignment with the target center. This indicator, which is distinct from the IOU, guides the frequency passband to move closer to the central frequency.

These three indicators can be combined in a linearly weighted manner to form a comprehensive reward function:

$$R_t = IOU + 10 \times (6 + \max s_{21}) - |DC - TC| \quad (1)$$

where  $s_{21}$  denotes the frequency response function, which represents the gain or attenuation between different frequency signals and their responses; DC indicates the central frequency of the current circuit; and TC refers to the expected central frequency of the circuit design. We stipulate that the insertion loss of the filtering circuit should be less than 6 dB for a

normal working frequency passband. As is less than 6 and the IOU range is  $[0, 100]$ , the insertion loss is multiplied 10 times to augment the impact of insertion loss on the rewards. Thus, the frequency passband overlap range, insertion loss, and frequency concentration, could be comprehensively assessed while conducting parameter optimization. Moreover, we dynamically adjusted the weights of the three components, initially optimizing the insertion loss to acquire circuit design schemes that may not satisfy the requirements but can function normally, then directing the working central frequency toward the desired one, and finally reinforcing the IOU to obtain feasible solutions. Additional penalties are imposed on invalid designs. Furthermore, the reward is gradually lowered during training to prevent overfitting. Following sufficient training, the intelligent agent learns strategies for configuring circuits that satisfy various criteria. Evaluation of the central frequency deviation is an innovative aspect of the reward function. In addition to considering the degree of frequency passband overlap, it is important to match the central frequency. We aim to encourage the intelligent agent to acquire the ability to regulate the frequency passband distribution centrally by introducing a central frequency deviation. The intelligent agent can modify the concentration of the frequency passband distribution by adjusting the resonator parameters when the deviation in the central frequency is adjusted. Thus, when faced with newly set desired central frequencies, the intelligent agent can quickly configure the corresponding circuit parameters, aligning the response with the desired central frequency without the need to retrain from scratch.

#### D. Intelligent Agent Design

Policy and value networks are the core components of an intelligent agent. The policy network generates the probability distribution of the actions to be taken given a particular state. In the proposed approach, the policy network includes an input layer, two hidden layers, and an output layer. The input layer receives representations of the geometric circuit parameters. The number of nodes is equal to the dimensionality of the state representation. The first hidden layer includes 256 fully connected nodes, each connected to all nodes of the input layer. It introduces nonlinearity through a rectified linear unit activation function to extract advanced-state features. Similarly, the second hidden layer contains 256 fully connected nodes connected to all nodes of the first hidden layer. The number of nodes in the output layer corresponds to the action space. A Softmax activation function transforms the value of each node into its corresponding action probability. This multi-layer, fully connected network structure effectively integrates state feature learning and action probability output. This policy-network structure is widely adopted for RL. Furthermore, to enhance the generalization capability of the network, the first hidden layer includes a dropout operation that randomly masks certain nodes to prevent overfitting. The value network evaluates the long-term return of each state-action combination and outputs the corresponding state-action value. The value network adopts a similar multilayer, fully connected structure. It uses the geometric parameter representation of the circuit as the input and predicts the state-action value using two hidden layers.

#### E. Environment Design

It is difficult to design and construct a training environment when RL methods are employed to address novel problems. Building an entirely new environment presents significant challenges compared with applying methods to existing environments. First, it requires abstracting the target problem to determine the key elements, followed by appropriate simplification and mapping of complex problems into modelable Markov decision processes. Second, the environment should contain elements conducive to effective training. In addition, the environment must simulate the effects of various complex factors under real circumstances to enhance the generalizability of the model. Finally, an appropriate reward system must be devised. Only in well-designed environments can RL methods achieve their expected effectiveness.

1) *Environment Creation*: In a designed environment, a pivotal step is to provide a circuit-parameter configuration scheme for the initial state of the environment. Accordingly, we devised two approaches to obtain high-quality initial states.

The first approach is the BRI, which generates a circuit topology that reasonably satisfies the performance requirements. Specifically, we utilized CircuitGenerator [5] to generate 2000 circuit topologies randomly. The score for each structure was calculated as,

$$R_t = \text{IOU} + 10 \times (6 + \max s_{21}) \quad (2)$$

and the structure with the highest score was selected as the initial state of the environment. The proposed method continuously optimizes the generated initial circuit topology, reducing the memory consumption and improving efficiency.

Another approach involves manually specifying the initial state of an environment. This method enables the use of circuit topologies designed manually by electronic engineers based on their experience as the initial state of the environment. It also permits further optimization based on the previous round of optimization, as detailed in Section III-F.

2) *Environment Control*: In the designed circuit optimization environment, the action space is discrete and different sensitivity levels exist for the optimized parameters. The magnitude of the changes in these parameters causes varying degrees of state transitions owing to the different actions taken, leading to disparate results. Therefore, a robust state-control strategy must be developed. Effective state control ensures a smooth progression of the training process. The value of delta is set to 0 as the base change factor for all operable parameters. The primary logic for state control is as follows: Initially, the environment maintains a triplet comprising the initial circuit state, initial circuit frequency response  $s_{21}$ , and initial circuit reward. Similarly, it maintains another triplet comprising the current circuit state, current circuit frequency response  $s_{21}$ , and current circuit reward. When the agent performs a new action, the horizontal and vertical positions of the resonators are less sensitive to numerical variations. In this study, the amplitude change factor was set to 1. The side length and thickness of the resonator cavity are relatively sensitive to numerical variations and were thus assigned an amplitude change factor of 0.5. The counterclockwise angle  $u$  from the horizontal line to the

line connecting the opening position and the center point was the most sensitive to numerical variations. Thus, its amplitude change factor was set to 0.01 and could be changed cyclically. We ensured that upon altering  $u$ , its value fell within the range of  $[0, 1]$  by adjusting it through periodic increments or decrements. Subsequently, the environment verifies the validity of the new state. For parameter conflicts, the environment applies a negative reward penalty based on an IDP policy. The valid states are subjected to a performance evaluation. Step rewards are computed based on the current state reward and the reward before the change. Moreover, the environment manages the initiation and termination of training episodes. Once an episode begins, the environmental state is initialized. Specifically, during the first call of the initialization method, the BRI method generates a circuit topology as the initial state. Throughout the iterative optimization of the parameters by the agent, the environment assesses whether the optimization objective has been achieved. If achieved, it concludes the current episode and triggers the storage module to save important training data for this iteration, including the state sequence, rewards, and total rewards. The corresponding data serve algorithm optimization and analysis purposes.

3) *Performance Evaluation*: In RL tasks, the environmental assessment of the state performance determines the efficacy of the agent. Supervised learning relies on labelled datasets. In contrast, the only feedback to the RL during training is the environmental reward. Therefore, the quality of the environment determines the RL efficacy. An accurate assessment module for the circuit performance must be established when designing an environment. The evaluation indicators must comprehensively consider various performance dimensions while requiring precise weight adjustments. Furthermore, invalid designs that could otherwise mislead the learning process must be identified and penalized. This approach ensures that the learning process obtains the correct and efficient policies only when the environmental evaluation mechanism is sufficiently reliable and accurate. We designed a performance evaluation function for the environment as follows. Specifically, we predicted  $s_{21}$  for the current circuit parameter configuration by utilizing the forward prediction module of CircuitGNN [5]. Subsequently, we calculated the passband IOU based on  $s_{21}$  and considered the maximum value of  $s_{21}$  as the insertion loss of the current scheme for circuit parameter optimization. The frequency at which  $s_{21}$  reaches its maximum value becomes the working central frequency of the current scheme for circuit parameter optimization. We aimed for this evaluation method not only to optimize single-frequency passband design, but also to address challenges posed by the optimization of multi-frequency passband design. For a single-frequency passband, the IOU calculation is relatively simple and only involves intersecting and comparing the delivered frequency passband with the expected frequency passband. However, multi-frequency passband IOU calculations are more intricate, as interactions between the frequency passbands must be handled. Specifically, when optimizing multiple frequency passbands simultaneously, calculating the IOU separately for each passband and performing averaging is inadequate. One challenge is that the delivered frequency passband of the

circuit may not entirely overlap with the expected frequency passband; instead, partial overlap can occur. In the delivered circuit, any frequency passband that does not overlap with the target circuit is considered ineffective. Simple IOU calculations may be erroneously included within the effective overlap range. Another challenge is managing the distance relationships between the frequency passbands. Long inter-band intervals offer no benefit to model learning, requiring the consideration of penalties or adjustments to the frequency passband weights. The frequency passband positions must also be managed properly. If multi-frequency passbands are included in the same region, then the problem of repeated calculations must be addressed. To address this problem, we propose a dynamic programming algorithm for calculating the multi-frequency passband IOU.

---

#### Algorithm 1

**Input:**  $X$ : the list of effective frequency passbands for the current designed circuit;  $Y$ : the list of frequency passbands for the expected circuit;  $L_X$ : the length of  $X$ ;  $L_Y$ : the length of  $Y$

**Output:** Multi-frequency passband IOU

```

1: Initialize a zero-array IOUs of size  $(L_X + 1) \times (L_Y + 1)$ 
2: for  $i = 1, \dots, L_X$  do
3:   for  $j = 1, \dots, L_Y$  do
4:     Compute the single-frequency passband intersection  $I = \text{Pass}_i \cap \text{Pass}_j$ 
5:     Compute the single-frequency passband union  $U = \text{Pass}_i \cup \text{Pass}_j$ 
6:     if  $U > 0$  then
7:        $\text{IOU} = I/U$ 
8:        $\text{IOUs}[i, j] = \max(\text{IOU}, \text{IOUs}[i - 1, j], \text{IOUs}[i, j - 1])$ 
9:     else
10:       $\text{IOUs}[i, j] = \max(\text{IOUs}[i - 1, j], \text{IOUs}[i, j - 1])$ 
11:    end if
12:   end for
13: end for
14: return  $\text{IOUs}[L_X, L_Y]$ 

```

---

#### F. End-to-End DFC Design Automation

To fully automate the end-to-end generation of circuit schemes from design objectives, we developed an efficient and stable RL-based method that considers the effectiveness, flexibility, and diversity within a discrete action space. The system was established by integrating comprehensive state representations and reward mechanisms and operates solely based on the input of the expected frequency passband. Our approach entails two key stages: rapid, stable, and high-quality initialization, followed by meticulous step-by-step optimization. In the initial stage, the BRI rapidly generates multiple circuit topologies. The optimal topology is then selected using a performance evaluation function, which serves as the starting point for the subsequent optimization. Our end-to-end automated design method does not require a highly specific initial state for the circuit and can iteratively progress from

a particularly poor initial state to achieve an excellent circuit design. The second stage performs step-by-step optimization using deep RL. We trained an RL intelligent agent, RLDFCDO, that interacts with a circuit simulation environment akin to an experienced electronic engineer in the real world. It adjusts the parameters incrementally based on performance feedback, gradually approaching the target frequency response. We encapsulated this agent as a callable module that could be seamlessly embedded into the automation process, enabling fine-grained automatic optimization. Moreover, we designed a comprehensive control logic that autonomously generated the initial states from the initialization model BRI and imported them into RLDFCDO for iterative optimization. Additionally, we developed a performance indicator monitoring and evaluation mechanism to terminate iterations actively and output the final results. The combination of efficient prior-driven initialization and stable RL optimization resulted in an end-to-end closed-loop automation process.

## IV. RESULTS

### A. Benchmarks and Settings

We implemented the PPO algorithm using PyTorch [46] and constructed a circuit optimization environment named *FilterEnv* based on the forward pre-trained model of CircuitGNN [5]. The circuit performance was evaluated based on the weighted sum of the IOU and insertion loss (Eq.2). All the validation experiments used a consistent learning rate of  $7 \times 10^{-4}$  and were conducted on an NVIDIA GeForce RTX 3090 GPU with 24 GB VRAM. The number of random seeds was set to 8 before each experiment. Importantly, all the experimental results were reproducible.

### B. Ablation Studies

We randomly selected four expected single-frequency passband targets: (240, 250), (250, 270), (270, 300), (300, 340); and four expected dual-frequency passband targets: [(240, 250), (300, 310)], [(240, 260), (300, 320)], [(240, 270), (300, 330)], [(240, 280), (300, 340)]. Three types of ablation studies were conducted using a type 2 DFC topology comprising four resonators [5]. The initial states before optimization were generated using the BRI method.

1) *Action Space*: To validate the effectiveness of our chosen action space, we conducted an ablation study involving 31 combinations (listed in Table I) comprising parameters  $x$ ,  $y$ ,  $a$ ,  $w$ , and  $u$  of the resonators as potential actions for the intelligent agent. The average change in the weighted sum of the IOU and insertion loss were measured before and after optimization for each combination, as depicted in Figs.3(a) and (b). This corroborates the discussion in Section III-B.

2) *IDP*: Generally, two strategies are employed to handle invalid actions. The first strategy ignores invalid actions, ensuring the perpetual legality of layout states. In the short term, this strategy is advantageous because it allows the agent to explore a greater state space. However, it fails to teach the model how to avoid such actions. In the long term, a considerable proportion of attempted actions become invalid. The second strategy is to penalize invalid actions. When an invalid action

is encountered, this strategy terminates the exploration of the agent and resets its environmental state. In the short term, the agent loses its ability to explore additional states. However, in the long term, the agent learns to avoid invalid actions. As the agent continues to learn, more invalid actions are avoided, increasing the number of exploration steps. We conducted an ablation study and compared the results with an invalid action-ignoring strategy to validate the effectiveness of the IDP strategy. The results are shown in Figs.3(c) and (d).

3) *Power of Step Reward*: In the initial stages of implementing the *FilterEnv* environment, we simply used the difference between the rewards before and after a step as the step reward. To encourage the model to learn to make steps that improve the state and avoid steps that worsen it, we conducted an ablation study on the power of the difference between the rewards before and after a step, denoted as  $r_1$  and  $r_2$ , respectively. In particular, if the layout state after the step was illegal, we followed the IDP strategy in Section III-E2 to set the step reward to  $-200^{power}$ . We conducted an ablation study by setting the power to 0, 1, 2, and 3 to avoid the potential risk of reward overflow owing to excessively large rewards.

$$\begin{aligned} \text{sign} &= \begin{cases} 1 & \text{if } r_1 < r_2 \\ -1 & \text{otherwise} \end{cases} \\ \text{step}_r &= \text{sign} \times (r_1 - r_2)^{power} \end{aligned} \quad (3)$$

The ablation results are displayed in Figs.3(e) and (f).

### C. Performance Evaluation

1) *Cumulative Distribution Function (CDF)*: We compared our method with the inverse optimization method proposed in CircuitGNN [5] by designing 1500 single-bandpass filtering circuits<sup>1</sup>. The bandwidths of the filtering circuits were randomly distributed between 10 and 80, as presented in Table II, whereas the center frequencies varied randomly between  $230 + \text{bandwidth}/2$  GHz and  $370 - \text{bandwidth}/2$  GHz.

We utilized three metrics to evaluate the quality of the designed filtering circuits across 1500 samples. The passband IOU metric assessed the alignment between the delivered passband and the expected passband, following the definition in Section 3.3. The insertion loss, as defined in [5], was calculated as the reciprocal of the maximum value of  $s_{21}$ . Lower insertion loss values indicate superior filtering circuit performance. The reward, as defined in Eq.2, was introduced to balance the importance of the IOU and the insertion loss. This metric provides a more comprehensive representation of the quality of filtering circuit design. Note that the circuits generated by the CircuitGNN method often have low insertion losses (good) and low passband IOUs (bad). We opted against the CircuitGNN method, which selects the layout scheme with the lowest train loss; instead, we compared our approach by selecting the layout with the maximum weighted sum of the passband IOU and insertion loss. The proposed method demonstrates superior circuit performance compared with CircuitGNN (Fig.4). First, the proposed method achieves

<sup>1</sup>Visualized comparison results of all 47 DFC topologies can be found in the supplemental information.

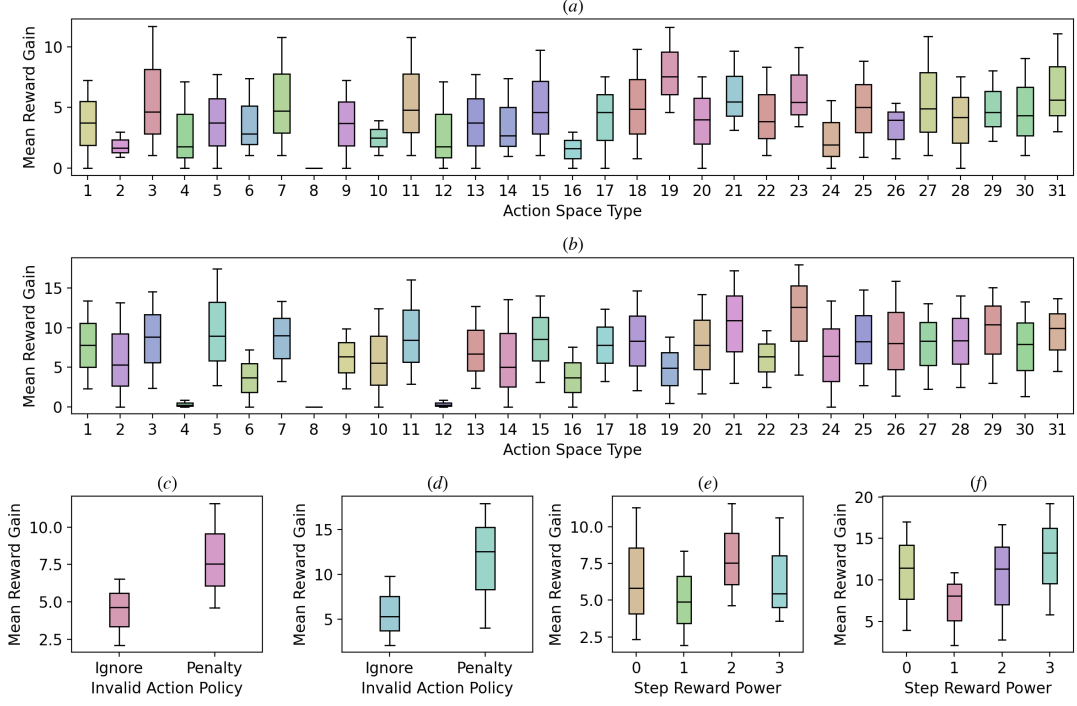


Fig. 3. Ablation study results. The central black lines in the boxes indicate the mean values. Average reward gains for 31 types of selectable action spaces across four (a) single- and (b) dual-frequency passbands. Average reward gains for the two invalid action strategies across the four (c) single- and (d) dual-frequency passbands. Average reward gains for four-step reward power variations across four (e) single- and (f) dual-frequency passbands.

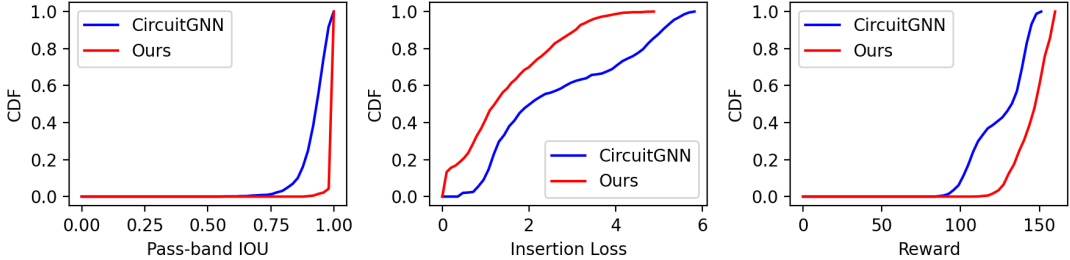


Fig. 4. Comparison of the CDFs of our method and CircuitGNN.

an average passband IOU that is notably higher than that of CircuitGNN. A high passband IOU signifies a good match between the passbands of the delivered filtering circuit and the expected design requirements. A high IOU implies a steep passband, which enhances the ability of the filtering circuit to reject signals from adjacent frequencies. Since our method attains high IOU metrics, it can yield filtering circuits with superior performance. In addition, the average insertion loss of our method is clearly reduced compared to that of CircuitGNN. The low insertion loss implies less attenuation of signals passing through the filtering circuit, resulting in higher quality. A lower loss leads to stronger signals at the receiving end, a lower signal-to-noise ratio, and improved reception performance. The insertion loss reduction also enables the transmission end to utilize a lower output power. Reducing the transmission power also reduces the power consumption of the system. Finally, considering the combined effect of IOU

and loss, our reward function score reached 145.18, whereas CircuitGNN scored 125.46, indicating a significant overall performance enhancement.

2) *Performance on All-Filtering Circuit Templates:* Five single-frequency bandpass filtering circuit design tasks were randomly selected, and optimization was performed using our proposed method and the inverse method proposed in CircuitGNN. Each single-frequency bandpass design task was executed across all five filtering circuit templates, and the average rewards for the different resonators and topologies were compared. As suggested by the results shown in Fig.5, the proposed method is advantageous compared to the CircuitGNN inverse method, consistently exhibiting superior performance and indicating its robustness in filtering circuit design tasks. Generally, a single-frequency bandpass filtering circuit design requires balancing conflicting objectives while maximizing the passband IOU. The proposed method realizes

TABLE I  
DIFFERENT TYPES OF SELECTABLE ACTION SPACES.

#Combination	State Space	Action Space	Operable Parameters	Description
1	(4, 1)	9	$x$	select $x$
2	(4, 1)	9	$y$	select $y$
3	(4, 2)	17	$x, y$	select $x, y$
4	(4, 1)	3	$l$	select $l$
5	(4, 2)	11	$x, l$	select $x, l$
6	(4, 2)	11	$y, l$	select $y, l$
7	(4, 3)	19	$x, y, l$	select $x, y, a$
8	(4, 3)	3	$w$	select $w, \text{gap}_h, \text{gap}_w$
9	(4, 4)	11	$x, w$	select $x, w, \text{gap}_h, \text{gap}_w$
10	(4, 4)	11	$y, w$	select $y, w, \text{gap}_h, \text{gap}_w$
11	(4, 5)	19	$x, y, w$	select $x, y, w, \text{gap}_h, \text{gap}_w$
12	(4, 4)	5	$l, w$	select $a, w, \text{gap}_h, \text{gap}_w$
13	(4, 5)	13	$x, l, w$	select $x, l, w, \text{gap}_h, \text{gap}_w$
14	(4, 5)	13	$y, l, w$	select $y, l, w, \text{gap}_h, \text{gap}_w$
15	(4, 6)	21	$x, y, l, w$	select $x, y, l, w, \text{gap}_h, \text{gap}_w$
16	(4, 3)	9	$u$	select $u, \text{gap}_x, \text{gap}_y$
17	(4, 4)	17	$x, u$	select $x, u, \text{gap}_x, \text{gap}_y$
18	(4, 4)	17	$y, u$	select $y, u, \text{gap}_x, \text{gap}_y$
19	(4, 5)	25	$x, y, u$	select $x, y, u, \text{gap}_x, \text{gap}_y$
20	(4, 4)	11	$l, u$	select $a, u, \text{gap}_x, \text{gap}_y$
21	(4, 5)	19	$x, l, u$	select $x, l, u, \text{gap}_x, \text{gap}_y$
22	(4, 5)	19	$y, l, u$	select $y, l, u, \text{gap}_x, \text{gap}_y$
23	(4, 6)	27	$x, y, l, u$	select $x, y, l, u, \text{gap}_x, \text{gap}_y$
24	(4, 6)	11	$w, u$	select $w, u, \text{gap}_h, \text{gap}_w, \text{gap}_x, \text{gap}_y$
25	(4, 7)	19	$x, w, u$	select $x, w, u, \text{gap}_h, \text{gap}_w, \text{gap}_x, \text{gap}_y$
26	(4, 7)	19	$y, w, u$	select $y, w, u, \text{gap}_h, \text{gap}_w, \text{gap}_x, \text{gap}_y$
27	(4, 8)	27	$x, y, w, u$	select $x, y, w, u, \text{gap}_h, \text{gap}_w, \text{gap}_x, \text{gap}_y$
28	(4, 7)	13	$l, w, u$	select $a, w, u, \text{gap}_h, \text{gap}_w, \text{gap}_x, \text{gap}_y$
29	(4, 8)	21	$x, l, w, u$	select $x, l, w, u, \text{gap}_h, \text{gap}_w, \text{gap}_x, \text{gap}_y$
30	(4, 8)	21	$y, l, w, u$	select $y, l, w, u, \text{gap}_h, \text{gap}_w, \text{gap}_x, \text{gap}_y$
31	(4, 9)	29	$x, y, l, w, u$	select $x, y, l, w, u, \text{gap}_h, \text{gap}_w, \text{gap}_x, \text{gap}_y$

TABLE II  
PASSBAND DISTRIBUTION OF THE FILTERING CIRCUITS USED IN THE EXPERIMENT.

Bandwidth	10-19 GHz	20-40 GHz	41-59 GHz	60-80 GHz
Number	500	200	300	500

effective tradeoffs, demonstrating its outstanding optimization capability. Additionally, as the number of resonators increases, the superiority of the proposed method becomes more pronounced. Hence, the proposed method can effectively handle intricate scenarios. Even with the same number of resonators, the proposed method exhibits superior performance across various topologies. For instance, with four resonators, the proposed method significantly outperforms the CircuitGNN inverse method across 15 different topologies that cover diverse coupling schemes and physical layouts between resonators. Thus, the proposed method is generally effective and adaptable to the specifics of each unique filtering circuit design template. Electronics engineers can use the proposed method to significantly reduce the time and computational costs required to achieve optimal designs. Consequently, more efficient optimization enables manufacturers to respond swiftly to market demands and technological innovations.

3) *Optimization Capability for Individual Circuits:* We employed the BRI method to generate the initial layouts for two, three, four, five, six, and eight resonators and the cor-

TABLE III  
COMPARISON OF THE OPERATIONAL EFFICIENCIES OF OUR METHOD AND CIRCUITGNN.

Platform	CircuitGNN	Ours
CPU (i7-8700T ES)	30 s/iteration	60 iteration/s
GPU (3090 24 GiB)	1.2 s/iteration	200 iteration/s

responding topologies (i.e., all filtering circuit templates) for five random single-frequency bandpass filtering circuit design tasks. These layouts served as the basis for optimization using both the proposed method and the CircuitGNN inverse method. Finally, the average reward changes for the different resonators and topologies of the five single-frequency bandpass filtering circuit design tasks were compared. In this optimization task, both our method and the CircuitGNN method utilized the same initial layout (Fig.6). The filtering circuits optimized using the proposed method exhibit marked improvements. These results demonstrate that the proposed stepwise optimization approach can continuously improve the design schemes of individual circuits. Thorough training enabled the model to assimilate the experiential knowledge of circuit performance improvements. Therefore, the proposed method automatically designs entirely new circuits and enables continual optimization from an engineer design base. With further enhancements, the proposed automated optimization system can evolve into an ideal auxiliary tool for electronic engineering applications.

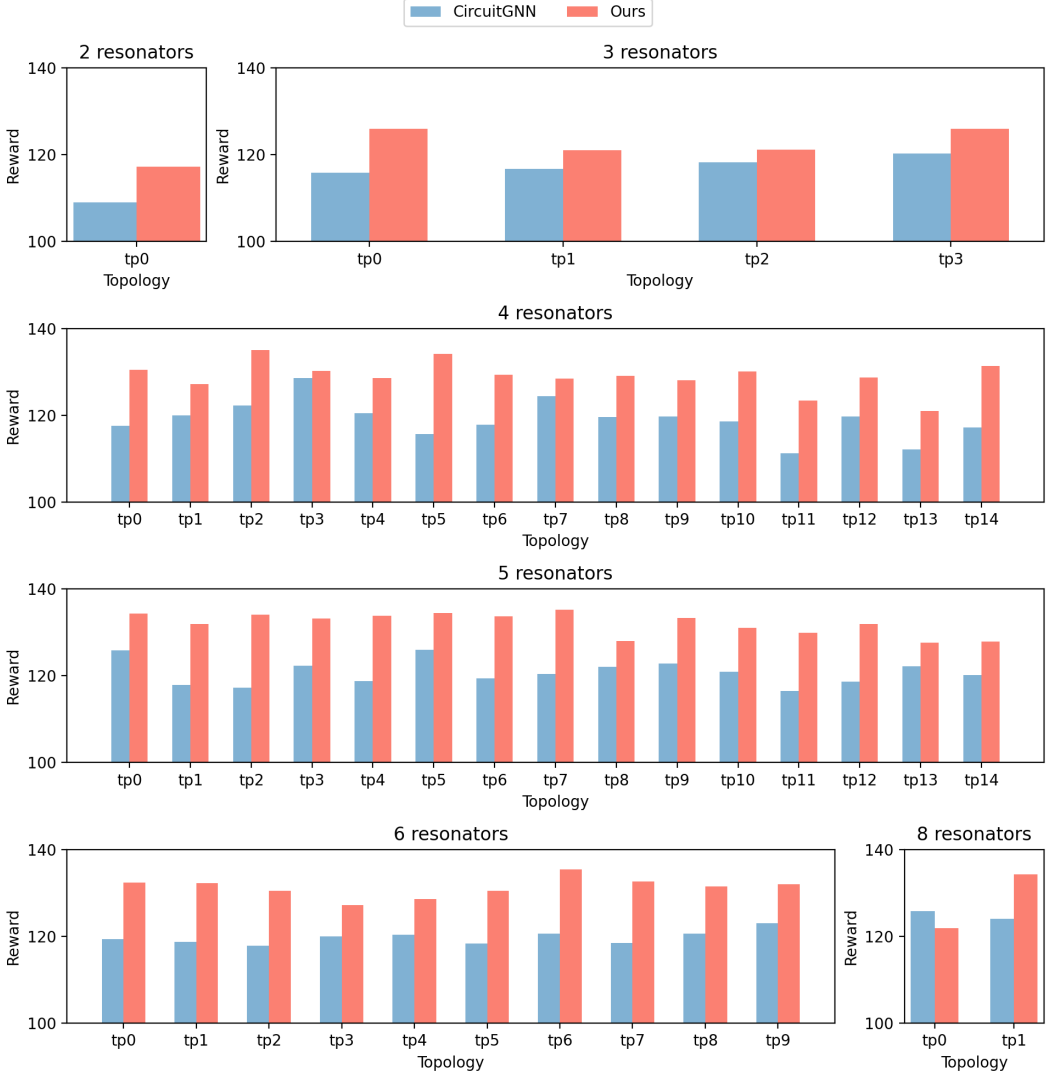


Fig. 5. Comparison of results between our method and the CircuitGNN inverse method in designing outcomes across all bandpass filtering circuit templates.

**4) Resource Utilization and Optimization Efficiency:** As derived from the results in Section IV-C3, the CircuitGNN inverse method [5] can concurrently optimize 2000 layouts. Thus, this technique demands a high memory with an average occupancy of 2460 MB, whereas the proposed method only requires 866 MB. The proposed method imposes low hardware-performance demands and achieves superior execution efficiency (Table III). Low resource utilization implies the potential deployment of our method on cost-effective hardware. By contrast, CircuitGNN requires high-end GPU platforms. Hence, the method proposed in this study significantly reduces machine costs. Furthermore, the proposed approach can optimize individual circuits while enhancing the computational efficiency. The training speed reaches approximately 60 iterations per second, which is 1800 times as fast as that of CircuitGNN. Overall, the proposed method can automatically optimize a single circuit efficiently and reliably using ordinary hardware by optimizing the computational process, thereby significantly enhancing the applicability of

TABLE IV  
COMPARISON OF PASSBAND IOU AND INSERTION LOSS RESULTS BEFORE AND AFTER OPTIMIZATION FOR FOUR DUAL-PASSBAND EXAMPLES USING OUR METHOD.

Expected passband	Passband IOU	Insertion loss
[(240, 250), (300, 310)]	73.22%/97.68%	5.13 dB/5.18 dB
[(240, 260), (300, 320)]	80.13%/95.45%	4.44 dB/4.46 dB
[(240, 270), (300, 330)]	76.70%/97.28%	2.81 dB/3.57 dB
[(240, 280), (300, 340)]	88.28%/91.75%	2.81 dB/2.78 dB

the proposed method in practical engineering and lowering the threshold for users to benefit from an automated design. The continual optimization of our automated design system could further reduce the demand for computational resources.

#### D. Multiple Passbands

Moreover, the proposed method demonstrates robust capabilities in simultaneously optimizing multiple passbands. Fig.7 illustrates the dual-passband cases, and Table IV presents

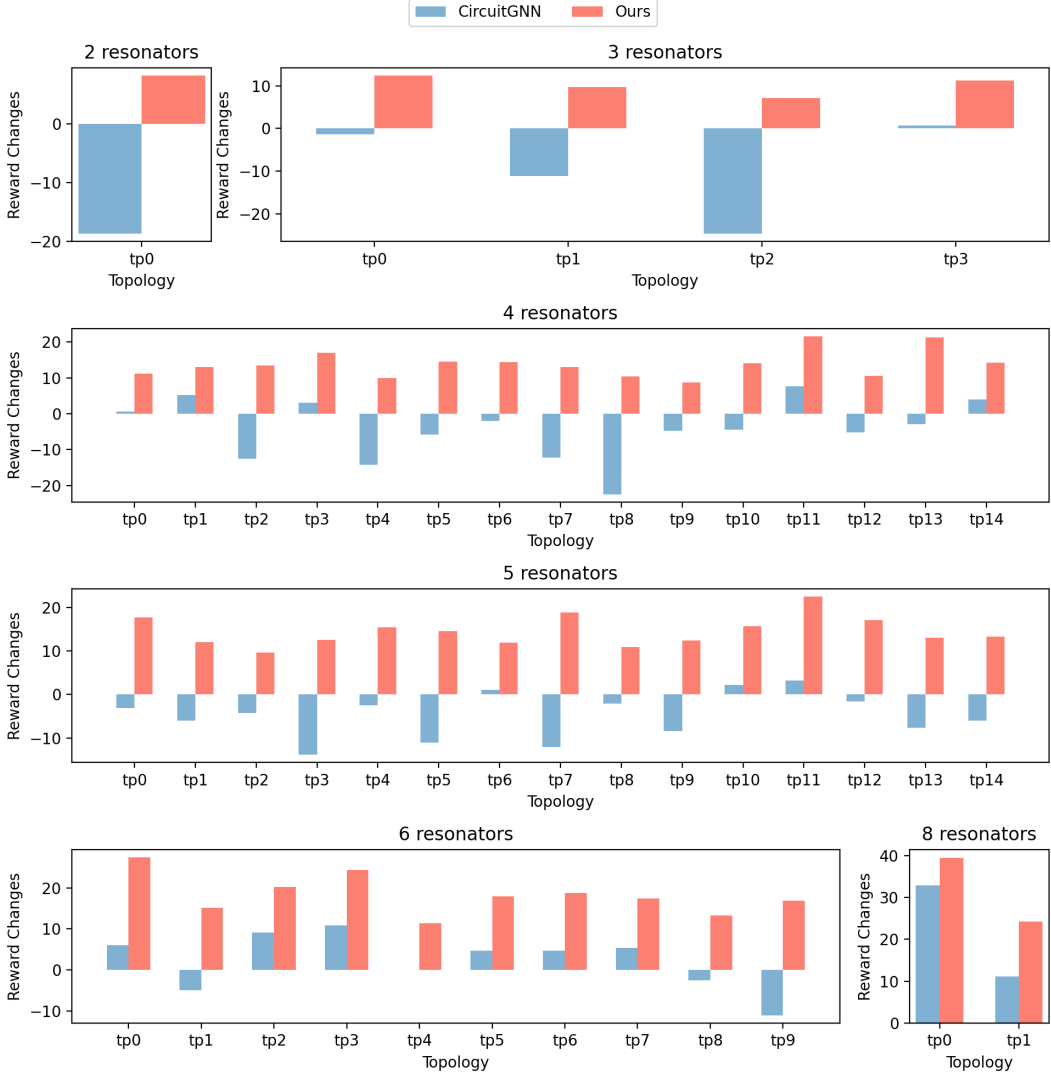


Fig. 6. Comparison of reward changes before and after optimization across all filter circuit templates between our method and the CircuitGNN method.

the specific data. Through optimization, the average passband IOU increased from 79.58% to 95.54%, with almost the same average insertion loss. Thus, the proposed method can effectively enhance the overall performance of multi-bandpass filtering circuits. The improvement in performance can be attributed to adopting an IOU metric that accurately reflects interactions across multiple passbands. As the number of frequency passbands increases, the complexity of the filtering circuit design increases exponentially. The proposed method offers a reliable and automated solution for the design of multi-bandpass filtering circuits. Through continual improvements, the proposed method can assist engineers in designing increasingly complex, multifunctional, and multifrequency filtering circuits.

## V. CONCLUSION

This study demonstrated the feasibility of using RL to optimize high-frequency filtering circuits and proposed an RL-based method for the automated optimization of DFCs. We

further developed an end-to-end solution for an automated DFC design by integrating BRI, significantly improving the efficiency of the design process and the reliability of the circuit performance. Compared with the existing methods, the proposed approach provides significant improvements. We extended the method to multi-bandpass filtering circuit design tasks and achieved outstanding results. The application of RL to circuit design not only enhances design accuracy, but also introduces new design paradigms in electronic engineering. However, several issues remain unresolved. First, better definition and evaluation of the multi-bandpass circuit performance are necessary. Second, the actions that can be performed are limited and may not accommodate non-standardized circuit design requirements. Moreover, we simplified the environmental space and used the geometric parameters of all the resonators comprising the filtering circuit as information for interaction with the intelligent agent. These measures lead to a loss of coupling information between resonators in the real world. Our future work will focus on addressing these limitations

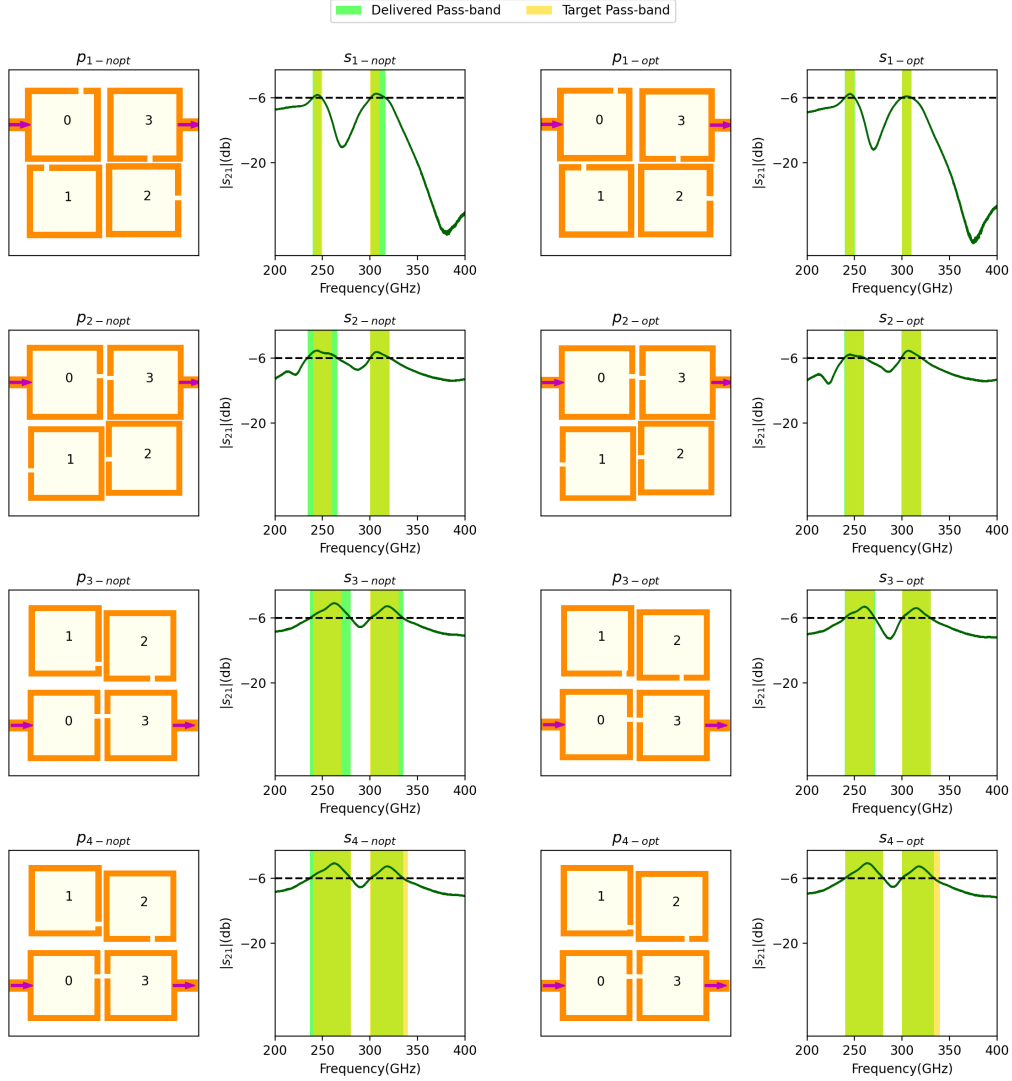


Fig. 7. Dual-passband optimization examples of four instances: layouts before and after optimization,  $s_{21}$ , and passband. Here,  $p_i-nopt$  and  $s_i-nopt$  respectively represent the  $i$ -th layout and performance ( $s_{21}$  and passband) before optimization, whereas  $p_i-opt$  and  $s_i-opt$  represent the layout and performance ( $s_{21}$  and passband) after optimization.

to achieve more comprehensive model structures, training methods, and benchmarks. We may employ graph structures to express the resonator features and coupling relationships. Moreover, we will attempt to optimize the rewards designed for multi-passband tasks and continue expanding the action space to optimize the designs.

## REFERENCES

- [1] X. Zhang, M. Jia, L. Chen, J. Ma, and J. Qiu, "Filtered-ofdm-enabler for flexible waveform in the 5th generation cellular networks," in *2015 IEEE global communications conference (GLOBECOM)*. IEEE, 2015, pp. 1–6.
- [2] S. Roy and A. Chandra, "Interpolated band-pass method based narrow-band fir filter: A prospective candidate in filtered-ofdm technique for the 5g cellular network," in *TENCON 2019-2019 IEEE Region 10 Conference (TENCON)*. IEEE, 2019, pp. 311–315.
- [3] J. Lee, M. S. Uhm, and I.-B. Yom, "A dual-passband filter of canonical structure for satellite applications," *IEEE Microwave and wireless components letters*, vol. 14, no. 6, pp. 271–273, 2004.
- [4] J.-S. G. Hong and M. J. Lancaster, *Microstrip filters for RF/microwave applications*. John Wiley & Sons, 2004.
- [5] G. Zhang, H. He, and D. Katabi, "Circuit-gnn: Graph neural networks for distributed circuit design," in *International conference on machine learning*. PMLR, 2019, pp. 7364–7373.
- [6] J.-S. Hong and M. J. Lancaster, "Couplings of microstrip square open-loop resonators for cross-coupled planar microwave filters," *IEEE Transactions on Microwave Theory and Techniques*, vol. 44, no. 11, pp. 2099–2109, 1996.
- [7] D. M. Colleran, C. Portmann, A. Hassibi, C. Crusius, S. S. Mohan, S. Boyd, T. H. Lee, and M. del Mar Hershenson, "Optimization of phase-locked loop circuits via geometric programming," in *Proceedings of the IEEE 2003 Custom Integrated Circuits Conference, 2003*. IEEE, 2003, pp. 377–380.
- [8] B. Liu, Y. Wang, Z. Yu, L. Liu, M. Li, Z. Wang, J. Lu, and F. V. Fernández, "Analog circuit optimization system based on hybrid evolutionary algorithms," *Integration*, vol. 42, no. 2, pp. 137–148, 2009.
- [9] Y. Wang, M. Orshansky, and C. Caramanis, "Enabling efficient analog synthesis by coupling sparse regression and polynomial optimization," in *Proceedings of the 51st Annual Design Automation Conference*, 2014, pp. 1–6.
- [10] T. McConaghay, P. Palmers, M. Steyaert, and G. G. Gielen, "Trustworthy genetic programming-based synthesis of analog circuit topologies using hierarchical domain-specific building blocks," *IEEE Transactions on Evolutionary Computation*, vol. 15, no. 4, pp. 557–570, 2011.

[11] N. Lourenço and N. Horta, “Genom-pof: multi-objective evolutionary synthesis of analog ics with corners validation,” in *Proceedings of the 14th annual conference on Genetic and evolutionary computation*, 2012, pp. 1119–1126.

[12] W. Lyu, P. Xue, F. Yang, C. Yan, Z. Hong, X. Zeng, and D. Zhou, “An efficient bayesian optimization approach for automated optimization of analog circuits,” *IEEE Transactions on Circuits and Systems I: Regular Papers*, vol. 65, no. 6, pp. 1954–1967, 2017.

[13] W. Lyu, F. Yang, C. Yan, D. Zhou, and X. Zeng, “Batch bayesian optimization via multi-objective acquisition ensemble for automated analog circuit design,” in *International conference on machine learning*. PMLR, 2018, pp. 3306–3314.

[14] ——, “Multi-objective bayesian optimization for analog/rf circuit synthesis,” in *Proceedings of the 55th Annual Design Automation Conference*, 2018, pp. 1–6.

[15] H. He, G. Zhang, J. Holloway, and D. Katabi, “End-to-end learning for distributed circuit design,” in *Workshop on ML for Systems at NeurIPS*, 2018.

[16] Y. Cao, G. Wang, and Q.-J. Zhang, “A new training approach for parametric modeling of microwave passive components using combined neural networks and transfer functions,” *IEEE Transactions on Microwave Theory and Techniques*, vol. 57, no. 11, pp. 2727–2742, 2009.

[17] F. Feng, C. Zhang, J. Ma, and Q.-J. Zhang, “Parametric modeling of em behavior of microwave components using combined neural networks and pole-residue-based transfer functions,” *IEEE Transactions on Microwave Theory and Techniques*, vol. 64, no. 1, pp. 60–77, 2015.

[18] F. Feng, C. Zhang, J. Ma, Q.-J. Zhang *et al.*, “Parametric modeling of microwave components using adjoint neural networks and pole-residue transfer functions with em sensitivity analysis,” *IEEE Transactions on Microwave Theory and Techniques*, vol. 65, no. 6, pp. 1955–1975, 2017.

[19] F. Mir, L. Kouhalvandi, and L. Matekovits, “Deep neural learning based optimization for automated high performance antenna designs,” *Scientific Reports*, vol. 12, no. 1, p. 16801, 2022.

[20] Z. Li, J. Peng, Y. Mei, S. Lin, Y. Wu, O. Padon, and Z. Jia, “Quarl: A learning-based quantum circuit optimizer,” *arXiv preprint arXiv:2307.10120*, 2023.

[21] D. Krylov, P. Khajeh, J. Ouyang, T. Reeves, T. Liu, H. Ajmal, H. Aghasi, and R. Fox, “Learning to design analog circuits to meet threshold specifications,” in *International Conference on Machine Learning*. PMLR, 2023, pp. 17858–17873.

[22] C. J. Watkins and P. Dayan, “Q-learning,” *Machine learning*, vol. 8, pp. 279–292, 1992.

[23] R. S. Sutton, “Generalization in reinforcement learning: Successful examples using sparse coarse coding,” *Advances in neural information processing systems*, vol. 8, 1995.

[24] P. Stone, R. S. Sutton, and G. Kuhlmann, “Reinforcement learning for robocup soccer keepaway,” *Adaptive Behavior*, vol. 13, no. 3, pp. 165–188, 2005.

[25] L.-J. Lin and T. M. Mitchell, “Reinforcement learning with hidden states,” *From animals to animats*, vol. 2, pp. 271–280, 1993.

[26] V. Mnih, K. Kavukcuoglu, D. Silver, A. Graves, I. Antonoglou, D. Wierstra, and M. Riedmiller, “Playing atari with deep reinforcement learning,” *arXiv preprint arXiv:1312.5602*, 2013.

[27] H. Van Hasselt, A. Guez, and D. Silver, “Deep reinforcement learning with double q-learning,” in *Proceedings of the AAAI conference on artificial intelligence*, vol. 30, no. 1, 2016.

[28] Z. Wang, T. Schaul, M. Hessel, H. Hasselt, M. Lanctot, and N. Freitas, “Dueling network architectures for deep reinforcement learning,” in *International conference on machine learning*. PMLR, 2016, pp. 1995–2003.

[29] S. Levine, C. Finn, T. Darrell, and P. Abbeel, “End-to-end training of deep visuomotor policies,” *The Journal of Machine Learning Research*, vol. 17, no. 1, pp. 1334–1373, 2016.

[30] J. Heinrich and D. Silver, “Deep reinforcement learning from self-play in imperfect-information games,” *arXiv preprint arXiv:1603.01121*, 2016.

[31] X. Zhao, L. Zhang, Z. Ding, L. Xia, J. Tang, and D. Yin, “Recommendations with negative feedback via pairwise deep reinforcement learning,” in *Proceedings of the 24th ACM SIGKDD international conference on knowledge discovery & data mining*, 2018, pp. 1040–1048.

[32] V. Konda and J. Tsitsiklis, “Actor-critic algorithms,” *Advances in neural information processing systems*, vol. 12, 1999.

[33] V. Mnih, A. P. Badia, M. Mirza, A. Graves, T. Lillicrap, T. Harley, D. Silver, and K. Kavukcuoglu, “Asynchronous methods for deep reinforcement learning,” in *International conference on machine learning*. PMLR, 2016, pp. 1928–1937.

[34] J. Schulman, S. Levine, P. Abbeel, M. Jordan, and P. Moritz, “Trust region policy optimization,” in *International conference on machine learning*. PMLR, 2015, pp. 1889–1897.

[35] J. Schulman, F. Wolski, P. Dhariwal, A. Radford, and O. Klimov, “Proximal policy optimization algorithms,” *arXiv preprint arXiv:1707.06347*, 2017.

[36] J. Bueno, S. Maktoobi, L. Froehly, I. Fischer, M. Jacquot, L. Larger, and D. Brunner, “Reinforcement learning in a large-scale photonic recurrent neural network,” *Optica*, vol. 5, no. 6, pp. 756–760, 2018.

[37] E. Kaufmann, L. Bauersfeld, A. Loquercio, M. Müller, V. Koltun, and D. Scaramuzza, “Champion-level drone racing using deep reinforcement learning,” *Nature*, vol. 620, no. 7976, pp. 982–987, 2023.

[38] T. D. Kulkarni, K. Narasimhan, A. Saeedi, and J. Tenenbaum, “Hierarchical deep reinforcement learning: Integrating temporal abstraction and intrinsic motivation,” *Advances in neural information processing systems*, vol. 29, 2016.

[39] T. Sugiyama, N. Schweighofer, and J. Izawa, “Reinforcement learning establishes a minimal metacognitive process to monitor and control motor learning performance,” *Nature Communications*, vol. 14, no. 1, p. 3988, 2023.

[40] C. Barata, V. Rotemberg, N. C. Codella, P. Tschandl, C. Rinner, B. N. Akay, Z. Apalla, G. Argenziano, A. Halpern, A. Lallas *et al.*, “A reinforcement learning model for ai-based decision support in skin cancer,” *Nature Medicine*, vol. 29, no. 8, pp. 1941–1946, 2023.

[41] P. Guo, K. Xiao, Z. Ye, H. Zhu, and W. Zhu, “Intelligent career planning via stochastic subsampling reinforcement learning,” *Scientific Reports*, vol. 12, no. 1, p. 8332, 2022.

[42] H. Ju, R. Juan, R. Gomez, K. Nakamura, and G. Li, “Transferring policy of deep reinforcement learning from simulation to reality for robotics,” *Nature Machine Intelligence*, vol. 4, no. 12, pp. 1077–1087, 2022.

[43] E. Kuprikov, A. Kokhanovskiy, K. Serebrennikov, and S. Turitsyn, “Deep reinforcement learning for self-tuning laser source of dissipative solitons,” *Scientific Reports*, vol. 12, no. 1, p. 7185, 2022.

[44] G. Dulac-Arnold, R. Evans, H. van Hasselt, P. Sunehag, T. Lillicrap, J. Hunt, T. Mann, T. Weber, T. Degrif, and B. Coppin, “Deep reinforcement learning in large discrete action spaces,” *arXiv preprint arXiv:1512.07679*, 2015.

[45] R. Dadashi, L. Huszenot, D. Vincent, S. Girgin, A. Raichuk, M. Geist, and O. Pietquin, “Continuous control with action quantization from demonstrations,” *arXiv preprint arXiv:2110.10149*, 2021.

[46] A. Paszke, S. Gross, F. Massa, A. Lerer, J. Bradbury, G. Chanan, T. Killeen, Z. Lin, N. Gimelshein, L. Antiga *et al.*, “Pytorch: An imperative style, high-performance deep learning library,” *Advances in neural information processing systems*, vol. 32, 2019.